ON THE STABILITY OF ROTATING MHD FLOWS

MARTY PH, MARTIN WITKOWSKI L,

TROMBETTA P AND TOMASINO T
Laboratoire LEGI
BP 53 X, 38041 Grenoble cedex, France
e-mail:Philippe.Marty@hmg.inpg.fr

AND

GARANDET J.P.
CEA-Grenoble
38054 Grenoble cedex 9, France

We present a numerical study of the flow induced by a rotating magnetic field on a liquid metal which fills a cylindrical container. Using a low frequency approximation and assuming axisymmetry, a finite difference technique is employed for the calculation of the flow field. Two different cases are considered in order to show that using a rotating magnetic field requires a detailed knowledge of its interaction with the flow. In the first situation, which is isothermal, it is shown that increasing the field intensity leads to the occurrence of Taylor-Couette type centrifugal instabilities depending upon the aspect ratio of the cavity. In the second case, which includes a heat transfer problem, it is shown that applying a very moderate rotating field to an initially unstable thermally driven convection is able to restore the flow stability.

1. Introduction

It is now admitted that applying a rotating magnetic field (RMF) may have, under particular circumstances, the effect of stabilizing an initially unstable flow. This property is of great interest in many respects, and particularly in crystal growth technology. Recent experimental works support this idea like the one made in Riga by Professor Gelgat's group (Gelfgat *et al*, 1996) or in Germany (see Dold and Benz 1995). As an example, in figure 1 published by these authors, one clearly show the effect of a limited magnetic field on the dopant striations in the solidified crystal.

A.Alemany et al. (eds.),
Transfer Phenomena in Magnetohydrodynamic and Electroconducting Flows, 327-343.

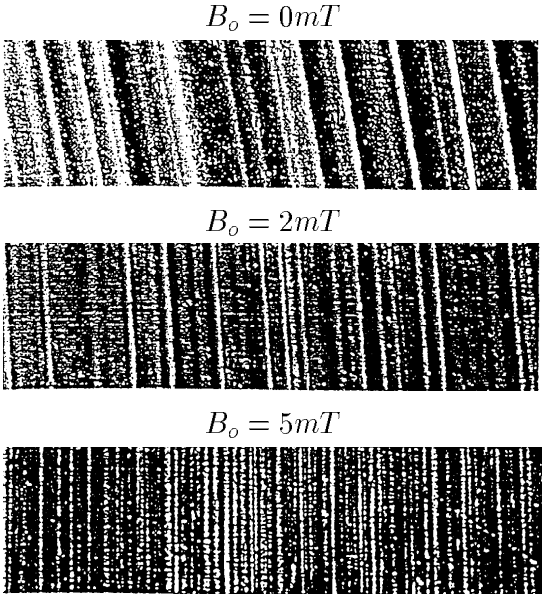

Figure 1. Decrease of the dopant striations when a rotating magnetic field is applied. Experimental results from P.Dold *et al* 1995 (the size of the samples is approx. $160 \times 630\ \mu m$)

These results have given a renew of interest to the topic of RMF for at least two reasons: on the one hand, creating a RMF device requires only a small amount of room and of electrical energy (what can be of great interest for space applications); on the other hand, the recent works which have been done to control a flow by means of a *dc* magnetic field have made clear the point that a rather heavy device had to be used in order to reach the required magnetic field. Up to now, no clear theoretical explanation or numerical demonstration have been given to explain or to illustrate the detailed action of a RMF on a fluid or thermal instability. It is precisely the aim of this paper to study the stability of a rotating flow driven by a RMF of limited frequency. Section 2 describes the model which has been used. The method for solving the electromagnetic force field is described in section 3. Section 4 gives the base flow solution in an isothermal situation. The results allow to determine the hydrodynamic stability diagram as a function of the magnetic Taylor number, T_m, and the aspect ratio of the cylindrical container. This is described in section 5. Section 6 studies a situation which is directly connected to the real crystal growth technology where unavoidable radial temperature defects are responsible for a thermally driven convection loop which instabilities can be damped by the use of a RMF.

2. Mathematical model

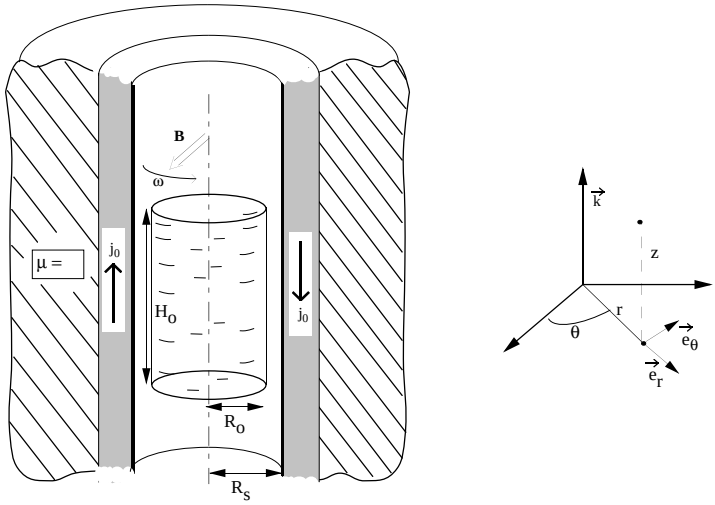

Figure 2. Geometry

We consider an isothermal, incompressible, viscous, electrically conducting fluid, contained in an electrically insulating truncated circular tube (radius R_o, height H_o) as shown in Fig. 2. The ratio H_0/R_0 is denoted by h. The properties of the fluid represented by the density ρ, the kinematic viscosity ν, the permeability μ and the conductivity σ are assumed to be constant. The fluid is submitted to the magnetic field created by an infinitely long surface current sheet located on the cylinder surface in $r = R_s > R_o$: $\vec{j} = -j_o \cos(p\theta - \omega t)\vec{k}$ where j_o is the lineic current density, $2p$ is the number of poles of the field and ω stands for the electric pulsation. The screening (or shielding) parameter $R_\omega = \mu\sigma\frac{\omega}{p}R_0^2$ is small compared to unity. The region $r > R_s$ is filled with a material of infinite permeability. We use the cylindrical coordinates (r, θ, z) associated to units vector ($\vec{e_r}$, $\vec{e_\theta}$, $\vec{k}$). The following characteristic scales have been used: $l_o = R_o$ for length, $\varphi_o = \frac{\omega}{p}B_oR_o^2$ for electric potential, $f_o = \sigma\frac{\omega}{2p}R_oB_o^2$ for electromagnetic forces. The velocity scale is denoted by U^* and its value will be precised later on according to the nature of the problem to be solved. The time scale t_o is R_o/U^*.

3. Electromagnetic force field

In the low frequency approximation ($\mu\sigma\frac{\omega}{p}R_o^2 \ll 1$) the magnetic field is unperturbed by the load and its expression:

$$\vec{B} = B_0 \left(\frac{r}{R_0}\right)^{p-1} (\sin(p\theta - \omega t)\vec{e_r} + \cos(p\theta - \omega t)\vec{e_\theta}) \tag{1}$$

satisfies:

$$\Delta\vec{B} = 0 \tag{2}$$

In equation (1) B_0 is the maximum intensity of the magnetic field in $r = R_0$. $\vec{B}$ is two-dimensional and the vector potential $\vec{A}$, such as $\vec{B} = \vec{curl}\vec{A}$, has only a z component which is:

$$A_z = -\frac{r^p}{p}\cos\left(p(\theta - t)\right) \tag{3}$$

In this dimensionless expression B_0R_0 and p/ω have been used as characteristic values for the vector potential and for the time. The radius r is now dimensionless. Moreover, the electric field $\vec{E}$ is classically written:

$$\vec{E} = -\vec{\nabla}\varphi - \frac{\partial\vec{A}}{\partial t} \tag{4}$$

where $\frac{\omega R_0^2 B_0}{p}$ is used to make φ dimensionless. Assuming the velocity of the fluid being much smaller than the velocity of the field, Ohm's law reduces to:

$$\vec{j} = \sigma\vec{E} \tag{5}$$

Taking the divergence of equation (5) together with equation (3) yields the dimensionless equation of the electric potential:

$$\Delta\varphi = 0 \tag{6}$$

Looking for solutions such as:

$$\varphi = \Phi(r, z)\sin\left(p(\theta - t)\right) \tag{7}$$

gives:

$$\frac{\partial^2\Phi}{\partial r^2} + \frac{1}{r}\frac{\partial\Phi}{\partial r} - \frac{p^2}{r^2}\Phi + \frac{\partial^2\Phi}{\partial z^2} = 0 \tag{8}$$

The boundary conditions at the cylinder boundaries are:

$$\Phi)_{r=o} = 0 \qquad \frac{\partial\Phi}{\partial r}\Big)_{r=1} = 0 \qquad \frac{\partial\Phi}{\partial z}\Big)_{z=0} = \frac{\partial\Phi}{\partial z}\Big)_{z=h} = r^p \tag{9}$$

These conditions express the cancelling of the normal electric current at the cylinder boundaries. A separation of variables solution for Φ gives :

$$\Phi = \sum_{n=1}^{+\infty} \left\{ C_{1n} cosh(\lambda_n z) + C_{2n} sinh(\lambda_n z) \right\} J_p(\lambda_n r) \tag{10}$$

where J_p are the Bessel functions of the first kind and where the λ_n are such as $J_p'(\lambda_n) = 0$ whereas $sinh$ and $cosh$ stand for the hyperbolic sinus and cosinus, respectively.

The boundary conditions in $z = 0$ and $z = h$ give:

$$r^p = \sum_{n=1}^{+\infty} \lambda_n C_{2n} J_p(\lambda_n r) = \sum_{n=1}^{+\infty} \lambda_n \left\{ C_{1n} sinh(\lambda_n h) + C_{2n} cosh(\lambda_n h) \right\} J_p(\lambda_n r) \tag{11}$$

From (11) one obtains :

$$C_{1n} = \frac{C_{2n}(1 - cosh(\lambda_n h))}{sinh(\lambda_n h)} \tag{12}$$

and, after some manipulations one finds :

$$C_{2n} = \frac{2p}{\lambda_n \left(\lambda_n^2 - p^2\right) J_p(\lambda_n)} \tag{13}$$

The final solution for Φ becomes :

$$\Phi = \sum_{n=1}^{+\infty} \frac{2p J_p(\lambda_n r)}{\lambda_n \left(\lambda_n^2 - p^2\right) J_p(\lambda_n)} \quad \frac{cosh(\lambda_n z) - cosh(\lambda_n (h - z))}{sinh(\lambda_n h)} \tag{14}$$

From Ohm's law one deduce the time and space averaged azimuthal force :

$$f_\theta = r^{p-1} \left(-\frac{\partial \Phi}{\partial z} + r^p \right) \tag{15}$$

where the $1/2$ coefficient coming form the integration of the sin^2 function is rejected into the force scale $f_o = \sigma \frac{\omega}{2p} R_o B_o^2$ already presented in the previous section. Then, equation (15) can be written :

$$f_\theta = r^{p-1} \left(r^p - \sum_{n=1}^{+\infty} \frac{2p J_p(\lambda_n r)}{\left(\lambda_n^2 - p^2\right) J_p(\lambda_n)} \frac{sinh(\lambda_n z) + sinh(\lambda_n (h - z))}{sinh(\lambda_n h)} \right) \tag{16}$$

This expression extends the work from (Mazuruk *et al.*, 1997) which is valid for $p = 1$ only.

4. Base flow solution in the isothermal case

The flow equations are described in terms of vorticity $\Omega \cdot \vec{e_\theta} = \vec{\nabla} \wedge \vec{V}$, stream function ψ defined by $\vec{\nabla} \wedge (-\frac{\psi}{r} \cdot \vec{e_\theta}) = (u, 0, w)$ and angular momentum $\Gamma = rv$:

$$\frac{\partial \Omega}{\partial t} + \frac{\partial (u\Omega)}{\partial r} + \frac{\partial (w\Omega)}{\partial z} - \frac{\partial}{\partial z}\left(\frac{\Gamma^2}{r^3}\right) = \frac{1}{T_m^{1/2}}\left(\frac{\partial^2 \Omega}{\partial r^2} + \frac{1}{r}\frac{\partial \Omega}{\partial r} - \frac{\Omega}{r^2} + \frac{\partial^2 \Omega}{\partial z^2}\right) \tag{17}$$

$$\frac{\partial^2 \psi}{\partial r^2} - \frac{1}{r}\frac{\partial \psi}{\partial r} + \frac{\partial^2 \psi}{\partial z^2} = r\Omega \tag{18}$$

$$\frac{\partial \Gamma}{\partial t} + \frac{\partial (u\Gamma)}{\partial r} + \frac{u\Gamma}{r} + \frac{\partial (w\Gamma)}{\partial z} = \frac{1}{T_m^{1/2}}\left(\frac{\partial^2 \Gamma}{\partial r^2} - \frac{1}{r}\frac{\partial \Gamma}{\partial r} + \frac{\partial^2 \Gamma}{\partial z^2}\right) + r f_\theta \tag{19}$$

where $T_m = (\frac{U^* R_o}{\nu})^2$. The velocity U^* is chosen equal to $\sqrt{\sigma\omega/2(p\rho)} B_o R_o$ and results from an equilibrium between the inertial forces and the electromagnetic forces. Then, the Taylor number becomes $T_m = \frac{\sigma\omega B_o^2 R_o^4}{2p\rho\nu^2}$. The equations (17) to (19) are solved numerically by using a second order finite difference scheme derived from (Sørensen *et al.*, 1989). The azimuthal force also contains a periodic component but we assume that it doesn't affect the flow as far as the fluid velocity is negligible compared to the velocity of the magnetic field (Davidson *et al.*, 1987) when the flow is dominated by inertia or as far as $\frac{\omega R_o^2}{p\nu} \gg 1$ when the flow is viscous dominated (see (Priede, 1993)).

Consequently, only the time-averaged value of the force (eq 16) is introduced in the momentum equation. This assumption can also be understood as follows: due to the equilibrium between the mean value $\sigma\frac{\omega}{2p} R_0 B_0^2$ of the electromagnetic forces and the inertial forces, the flow has a mean value U^* such as: $\sigma\frac{\omega}{2p} R_0 B_0^2 \approx \frac{\rho U^{*2}}{R_0}$. During a time interval of one electric period, $\frac{\omega}{p}^{-1}$, the flow experiences a fluctuation of the driving force of order $O(\sigma\frac{\omega}{2p} R_0 B_0^2)$. Again, a simple balance between this force and inertia writes: $\sigma\frac{\omega}{2p} R_0 B_0^2 \approx \rho\frac{\delta U^*}{(\omega/p)^{-1}}$ where δU^* stands for the fluctuating part of the velocity. Consequently, assuming the flow to be steady despite the fluctuating nature of the forces can also be written $\frac{\delta U^*}{U^*} << 1$ or, introducing an interaction parameter, N:

$$N = \frac{\sigma B_0^2}{\rho\omega} << 1 \tag{20}$$

This situation is quite at the opposite of that recently considered by (Walker, 1998) who studies the behavior of a flow driven by a RMF in a truncated liquid metal cylinder with $Ha >> 1$ and $N >> Ha$. Figure 3 shows the electric current lines for $H_0/R_0 = 0.66$. Their path is roughly vertical in the mid-height region , thus creating in this part a maximum value of the azimuthal force.

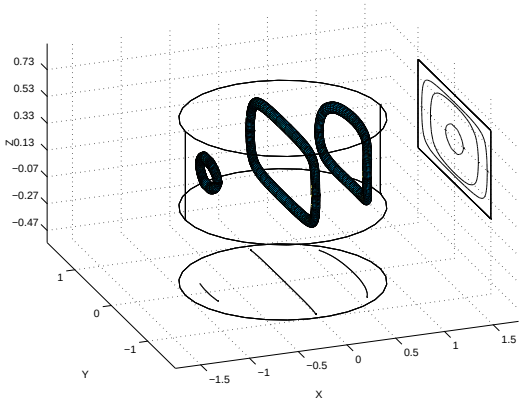

Figure 3. Electric current lines for $H_0/R_0 = 0.66$. At the instant when this plot has been made, the magnetic field is normal to y = constant planes.

The distributions of the azimuthal force f_θ is shown in Fig 4 for different aspect ratio of the cylinder. One notes that for $H_0/R_0 > 3$, the force distribution in the mid-plane becomes almost equal to that obtained in an infinitely long cylinder. Nevertheless, H_0/R_0 has to be greater than approximately 10 to allow the existence of a region near the mid-plane having an almost z-independent plateau.

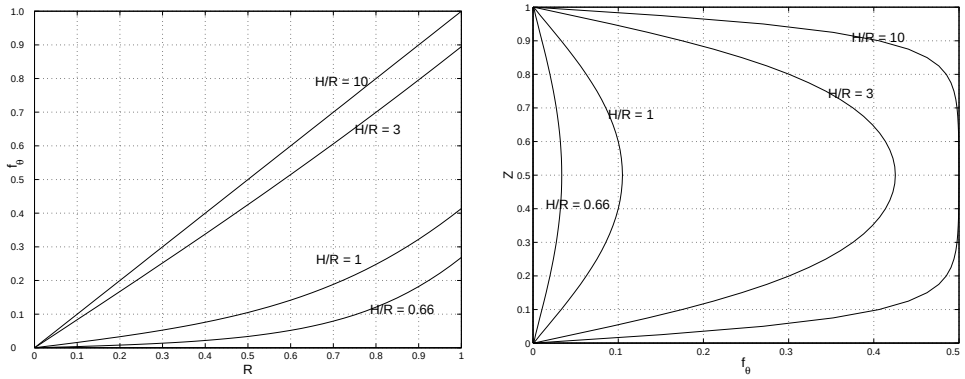

Figure 4. Radial and vertical distributions of the azimuthal force for different aspect ratio. a) $z = 0.5$ and b) $r = 0.5$.

Different flow regimes can be observed. For an aspect ratio $H_o/R_o = 2$, the influence of T_m on the flow has been studied in details. As T_m increases three flow regimes occur successively: a viscous regime, an inertial regime, an unstable regime. Gelfgat (1994) predicted a fourth regime where the flow again becomes

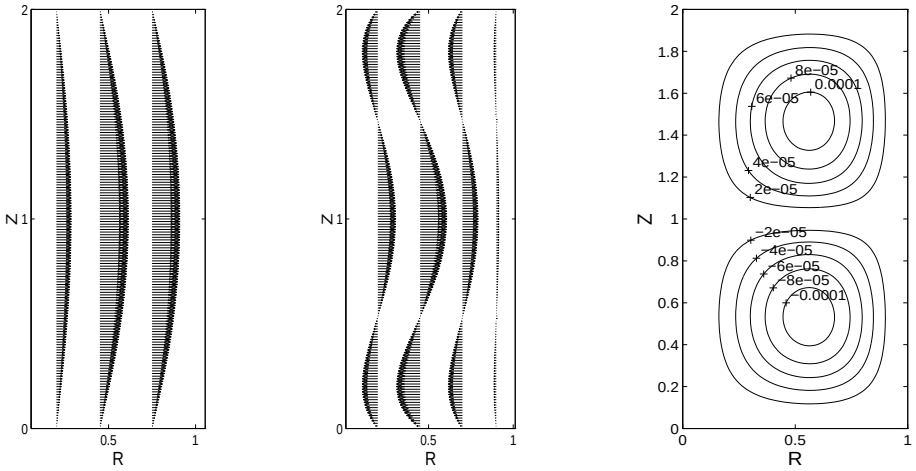

(a) (b) (c)

Figure 5. Velocity profiles at different radius and streamlines for a magnetic Taylor number $Tm = 10$ and an aspect ratio $H_o/R_o = 2$ (a) :Azimuthal velocity, v - (b) : Radial velocity, u (the length used for drawing the arrows is roughly 400 times larger than in (a)) - (c) : Meridional streamlines.

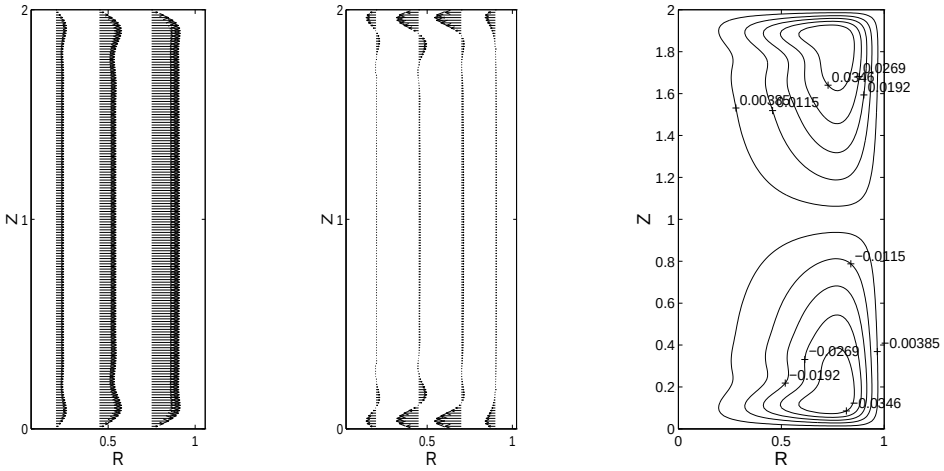

(a) (b) (c)

Figure 6. Velocity profiles at different radius and streamlines for a magnetic Taylor number $Tm = 10^5$ and an aspect ratio $H_o/R_o = 2$ (a) :Azimuthal velocity, v - (b) : Radial velocity, u (the length used for drawing the arrows is roughly the same as in (a)) - (c) : Meridional streamlines.

quasi stationary and stable but this prediction has not been observed in our numerical calculations.

In the viscous regime, the recirculating flow in the meridional plane has no effect on the angular momentum distribution which is controlled by an equilibrium between viscosity and the magnetic force. This can be written: $\mu v_\theta / R_0^2 \sim \sigma \frac{\omega}{2p} R_0 B_0^2$ or, in dimensionless form: $\frac{v}{U^*} \sim {T_m}^{1/2}$. The flow is shown on Fig 5. Both v or u have smooth profiles and no boundary layers appear. The meridional streamlines are almost circular.

In the inertial regime, the recirculating flow is strongly coupled with the azimuthal flow and by virtue of an analysis detailed in (Davidson, 1992) the order of magnitude of azimuthal velocity can be found: $\frac{v}{U^*} \sim {T_m}^{1/6}$. This situation is characterized by the existence of thin Ekman layers along the end walls in $z = 0$ and $z = h$ (see Fig 6). Most of the meridional recirculating flow passes through these layers where it looses the angular momentum picked up in the core due to the effect of its interaction with the electromagnetic forces. The thickness of the Ekman layers has the wellknown dimensionless value $\left(\frac{vR}{\nu}\right)^{-1/2}$ what can be written in dimensionless units:

$$\delta_{Ekman} \sim O(T_m^{-1/3}) \tag{21}$$

The radial velocity in these layers scales as the azimuthal velocity in the core, ie, $O(T_m^{1/6})$. The mass conservation of the recirculating flow gives the value of the meridional velocity in the core: $v_m(core) \sim O(T_m^{-1/6})$. Finally, on Fig 6, we can note an increase in v as one move from the core to the end walls. This is clearly a convective effect of the meridional flow which carries towards the center, fluid particles having a higher azimuthal velocity.

Figure 7 shows the evolution of the maximum value of the angular momentum in the whole fluid as a function of T_m. The slope found by the above calculations of order of magnitude matches reasonably well with our numerical calculations. It is clearly $1/2$ in the viscous regime for $T_m < 10^3$ and $1/6$ in the full inertial regime for $T_m > 10^5$. It is worth noting the existence of an intermediate region between $T_m = 10^3$ and $T_m = 10^5$ where v scales as $T_m^{0.3}$ but where the flow is still stable. This region probably allows a transition of the flow between the viscous and the inertial regimes. This latter becomes rapidly unstable if T_m increases. In figure 7, the last three points are already in the unstable regime. It is then surprising that the occurrence of flow instabilities does not affect the validity of an order of magnitude analysis which has nevertheless been made for a stable flow. The general tendency of these results is in agreement with those recently obtained by other authors(see (Priede, 1993) and (Davidson, 1992)).

5. Departure from stability due to the RMF action

The first stability study was performed by Richardson (Richardson, 1974). He showed the Taylor Couette like nature of the instability in the case of an infinite

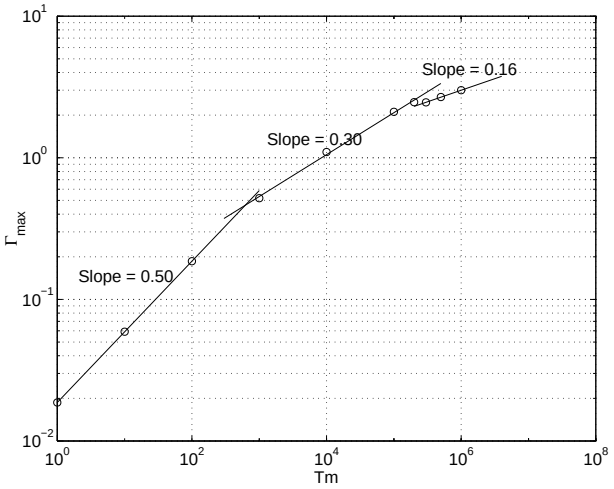

Figure 7. $H_o/R_o = 2$. Evolution of the maximum of angular momentum Γ_{max} in $[0, R_o]\times[0, H_o]$ vs magnetic Taylor number T_m

height. Gelfgat (Gelfgat *et al.*, 1994) found that the finite length of the cylinder was a stabilizing factor. For an aspect ratio $H_o/R_o = 2$, Gelfgat predicts the first transition for $T_m > 3.2 \cdot 10^5$ while for an infinite model the calculation gives $T_m = 2917$. In order to understand the mechanism of appearance of the instability and the effect of top and bottom end walls, we choose a sufficiently enhanced cylinder (aspect ratio $H_o/R_o = 10$). The exact determination of the transition threshold by means of direct simulation is a difficult task as the first perturbations are very weak and take a long time to appear. For the aspect ratio considered, we found that the critical T_m ranges in $[4050, 7200]$. The lower bound is obtained by decreasing T_m from the unstable regime till a stable regime is obtained while the upper bound is obtained doing the route backward. To illustrate the unsteady case, we choose therefore a regime where the oscillations are not too weak. On figure 8, we see the time evolution of the streamlines over one period and of a probe signal measuring the azimuthal velocity. As predicted by Richardson, we see the appearance of Taylor Couette vortices in the meridional plane created by the unstable part of the azimuthal velocity profile near the cylinder wall. The major difference between infinite case and the configuration of finite height is the fact that when unstable the flow is unsteady. The plane $z = H_o/2 = 5$ remains a plane of symmetry. The vortices are generated in the quasi z-independent zone of the cylinder and move from the plane of symmetry toward the extremities where they are destroyed. This is due to the presence of the Ekman pumping created by the end walls that attract the vortices. The signal shows this time evolution, each peak corresponding to a vortice passing in front of the probe.

It is interesting to draw the stability diagram of the evolution of the critical

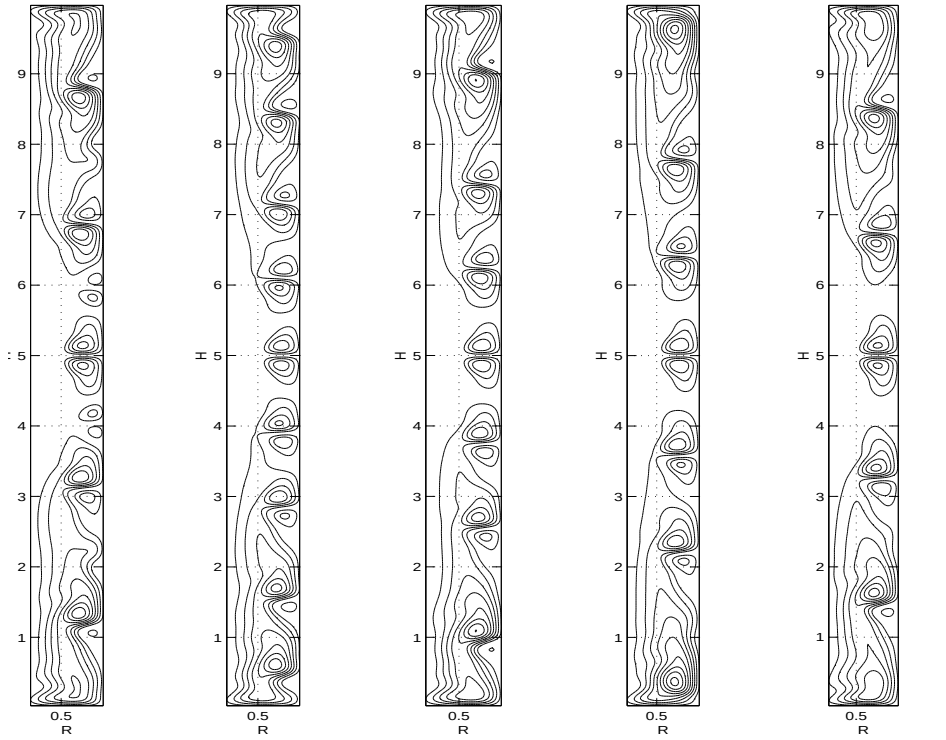

(a) T_o $T_o + 0.2 \cdot \Delta T$ $T_o + 0.4 \cdot \Delta T$ $T_o + 0.6 \cdot \Delta T$ $T_o + 0.9 \cdot \Delta T$

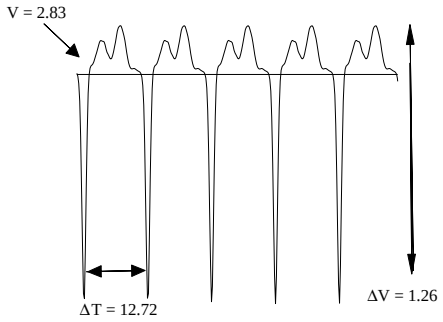

(b)

Figure 8. (a) Evolution of distribution of the stream function ψ over a period $\Delta T = 12.72$ for $T_m = 16200$, and $H_o/R_o = 10.(\psi \in [-0.157, +0.157]$ with 20 isovalues equally spaced). One can follow the evolution of a pair of vortices created at $z = 6$ ascending over $3 \cdot \Delta T$ toward the top wall and note the appearance of a pair of vortices at $z = 8.3$ for $T_o + 0.2 \cdot \Delta T$. (b) Signal of a probe measuring the azimuthal component of the velocity at $r = 0.85, z = 7.5$.

Taylor number vs the aspect ratio H_0/R_0. This is done in Fig 9. It is most probable that $(T_m)_{critical}$ will have an asymptotic dependence in $(H_0/R_0)^{-4}$ when $H_0/R_0 \to 0$. As a matter of fact, the -4 exponent eliminates the influence of the radius R_0, what is expectable when the cylinder height becomes vanishingly small compared to the radius.

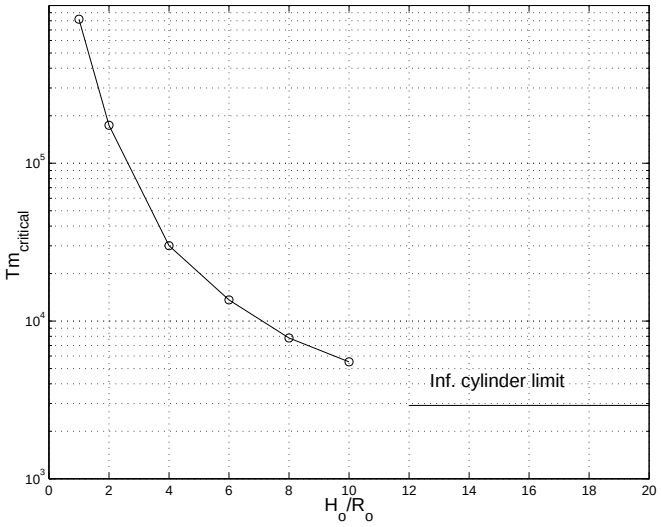

Figure 9. Evolution of the critical value of the magnetic Taylor number vs the aspect ratio H_0/R_0.

6. Recovering stable conditions with a RMF

The aim of this part is to explain the detailed mechanism by which a RMF may, under particular circumstances, contribute to stabilize an initially unstable flow. As many of the potential applications of this type of magnetic fields are connected with the crystal growth technology, it has appeared interesting to consider the situation described in Fig 10 where a cylindrical cavity is filled with a liquid metal which is possibly submitted to a rotating magnetic field. This situation is then close to the vertical Bridgman configuration.

The top boundary is at temperature $T_0 + \Delta T$ whereas a radial temperature defect due in practice to a difference between the thermal conductivities of the liquid and of the solid phase, is maintained along the bottom boundary in $z = 0$ where T is linearly increasing from T_0 in $r = 0$ to $T_0 + \epsilon\Delta T$ in $r = R$. The vertical wall is thermally insulated. Changing the parameter ϵ then allows to control the intensity of the thermally driven meridional flow in the (r, z) plane.The scale velocity U^* results from an equilibrium between buoyancy and inertial forces: $\rho g\beta\epsilon\Delta T \sim \rho U^{*2}/R_0$ where $\epsilon\Delta T$ is considered as being the significant quantity to estimate the buoyant effect and β is the thermal expansion coefficient. As a

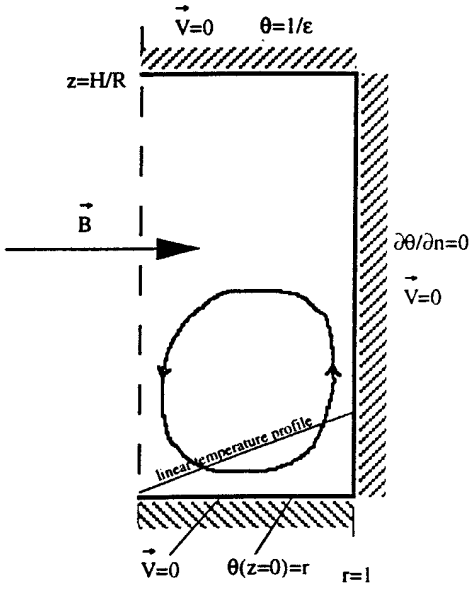

Figure 10. Test case for creating an initially unstable flow: a radial temperature distribution is imposed along the bottom wall of a cylindrical cavity having an adiabatic vertical wall and an isothermal top wall.

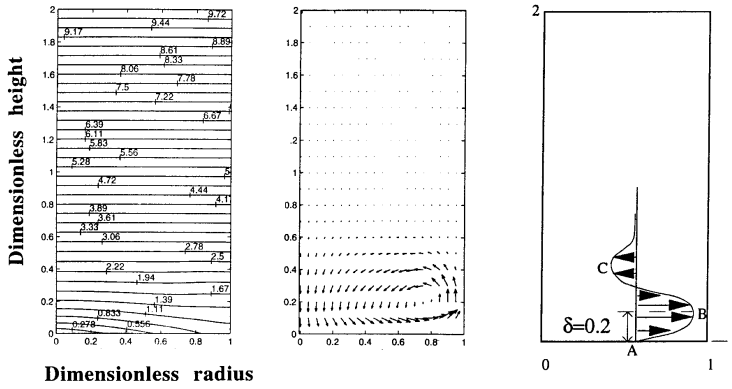

Figure 11. Temperature (a) and velocity (b and c) distributions for $\epsilon = 0.1$, $Pr = 0.01$, $Gr = 2.9\,10^6$ and $T_m = 0$.

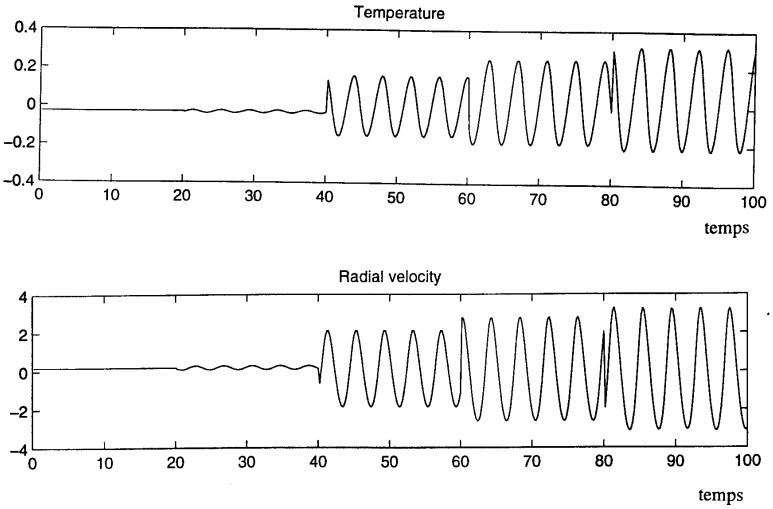

Figure 12. Time evolution of the temperature for $Gr = 3.1,\ 3.2,\ 3.5,\ 3.8$ and $4.1\ 10^6$ (Gr is increased in time every $\Delta t = 20$; the transient period between two successive values of Gr is not shown). $T_m = 0$, $H/R = 2$, $Pr = 0.01$ and $\epsilon = 0.1$.

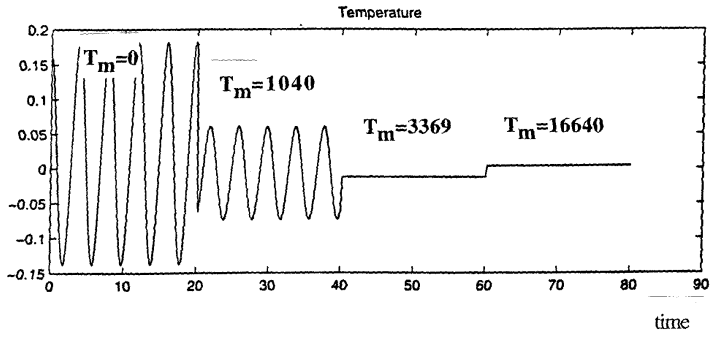

Figure 13. Temporal evolution of the temperature fluctuations in $r = 0.25$, $z = 0.2$ vs time for different T_m and for $Pr = 0.01$, $\epsilon = 0.1$, $Gr = 3.5\ 10^6$, $H/R = 2$. The transient period between two successive values of T_m is not shown.

result, the scale velocity U^* becomes equal to $\sqrt{g\beta\epsilon\Delta T R_0}$. Introducing a dimensionless temperature $\Theta = \frac{(T-T_0)}{\epsilon\Delta T}$, equations (17) to (19) and the energy equation become:

$$\frac{\partial\Omega}{\partial t}+\frac{\partial(u\Omega)}{\partial r}+\frac{\partial(w\Omega)}{\partial z}-\frac{\partial}{\partial z}\left(\frac{\Gamma^2}{r^3}\right) = \frac{1}{Gr^{1/2}}\left(\frac{\partial^2\Omega}{\partial r^2}+\frac{1}{r}\frac{\partial\Omega}{\partial r}-\frac{\Omega}{r^2}+\frac{\partial^2\Omega}{\partial z^2}\right)-\frac{\partial\Theta}{\partial r} \tag{22}$$

$$\frac{\partial^2\psi}{\partial r^2}-\frac{1}{r}\frac{\partial\psi}{\partial r}+\frac{\partial^2\psi}{\partial z^2} = r\Omega \tag{23}$$

$$\frac{\partial\Gamma}{\partial t}+\frac{\partial(u\Gamma)}{\partial r}+\frac{u\Gamma}{r}+\frac{\partial(w\Gamma)}{\partial z} = \frac{1}{Gr^{1/2}}\left(\frac{\partial^2\Gamma}{\partial r^2}-\frac{1}{r}\frac{\partial\Gamma}{\partial r}+\frac{\partial^2\Gamma}{\partial z^2}\right)+\frac{T_m}{Gr}rf_\theta \tag{24}$$

$$\frac{\partial\Theta}{\partial t}+u\frac{\partial\Theta}{\partial r}+w\frac{\partial\Theta}{\partial z} = \frac{1}{Pr\sqrt{Gr}}\left(\frac{\partial^2\Theta}{\partial r^2}+\frac{1}{r}\frac{\partial\Theta}{\partial r}+\frac{\partial^2\Theta}{\partial z^2}\right) \tag{25}$$

The Grashof and Prandtl numbers have their standard definitions:

$$Gr = \frac{g\beta\epsilon\Delta T R_0^3}{\nu^2} \qquad Pr = \frac{\nu}{\alpha} \tag{26}$$

The equations are solved using the same finite differences technique as that described in section 4.

When $T_m = 0$, Fig 11 shows the temperature and velocity distribution for $Gr = 2.9\ 10^6$, $Pr = 0.01$ and $\epsilon = 0.1$. The value 0.01 is a characteristic value of the Prandtl number of liquid metals whereas $\epsilon = 0.1$ corresponds to a radial temperature difference of $2K$ when a vertical temperature difference of $20K$ is applied between the top and bottom boundaries. The flow is confined at the bottom of the cell where the radial inhomogeneity of the temperature is important. It consists of a stationary radial jet along the bottom wall having an almost constant thickness $\delta \approx 0.2$. The flow stability is lost when Gr is increased (Fig 12). The amplitude A of the flow oscillations vs $Gr - Gr_c$ displays a Hopf bifurcation behavior. For $Gr = 3.5\ 10^6$, Fig 13 shows the damping of the temperature fluctuations when the magnetic Taylor number, T_m, is progressively increased from 0 to 16640.

A detailed study of the flow around the critical Grashof number Gr_c has shown that the bottom jet along the wall in $z = 0$ was responsible for the instability (Marty *et al.*, 1998). More precisely, the inflexional nature of its velocity profile is the dominant ingredient of this instability. For an unbounded geometry, such a profile is known to be unstable even for rather low Reynolds numbers (Villermaux, 1998). In our case, the dimensional confinement in the radial direction imposed by the vertical wall has the effect of preventing the perturbations having a wave-length greater than R to develop. This low-pass filtering is consequently

at the origin of a critical Reynolds number for the jet to which corresponds an associated critical Grashof number. Adding a rotation to the flow through electromagnetic azimuthal forces will generate a radial Ekman recirculating inward flow along both end walls. Along the bottom wall, this Ekman flow will then be opposite to the thermally driven flow and will thus lower the jet Reynolds number to a value situated below the critical threshold. This, in turn, will restore the flow stability.

7. Conclusion

A method of calculation of the flow induced by a low-frequency rotating magnetic field in a truncated liquid metal cylinder has been presented. In an isothermal cavity, the flow is found in agreement with calculations of other contributors: it consists of a viscous flow when the magnetic Taylor number, T_m, is lower than approximately 10^3 and of a flow dominated by inertia when T_m is greater than 10^5. In the viscous regime, the azimuthal velocity scales as $T_m^{1/2}$ whereas it scales as $T_m^{1/6}$ in the inertial regime. For various aspect ratios, the critical value of T_m which produces Taylor Couette instabilities in the flow has been found. The most important results of this study concerns the possibility to use a RMF to stabilize an initially unstable and time-dependent flow. This is of high practical interest for crystal growth technology. Although all these results show the promising future of RMF, they also illustrate how careful one has to be when this type of fields is considered for industrial applications. It is also likely that specific experimental studies on these flows should be undertaken in addition to the numerical approach.

References

DAVIDSON, P.A. and HUNT, J.C.R. Swirling recirculating flow in a liquid-metal column generated by a rotating magnetic field. *Journal of Fluid Mechanics*, 185:67–106, 1987.

DAVIDSON, P.A. Swirling flow in an axisymmetric cavity of arbitrary profile, driven by a rotating magnetic field. *Journal of Fluid Mechanics*, 245:669–699, 1992.

DOLD, P., and BENZ, K.W. Convective temperature fluctuations in liquid Gallium in Dependence on static and rotating magnetic fields, *Crystal Research Technology*, Vol.30, n.8, pp.1135–1145, 1995.

DOLD, P. , KAISER, Th., BOSCHERT, S. and BENZ, K.W., Modification of the heat transport by MHD-Flows in the vertical Bridgman crystal growth process, 8th Beer-Sheva Seminar on MHD Flows and Turbulence, 1995, Beer Sheva Conf., Israel.

GELFGAT, Y.M., GORBUNOV, L.A. and KOLEVZON, V. Liquid metal flow in a finite-length cylinder with a rotating magnetic field. *Experiments in Fluids*, 15:411–416, 1993.

GELFGAT, Y.M. and GORBUNOV L.A. Effect of alternating magnetic field on melt hydrodynamics in a cylindrical vessel with free surface. *Magnetohydrodynamics*, 30(3):237–247, 1994.

GELFGAT, Y.M., KRUMINS J., and ABRICKA A., On hydrodynamics, heat and mass transfer control in a cylindrical vessel by rotating magnetic field, *Proceedings of the 8th Bat-Sheva International Seminar*, 1996,Beersheva, Israel.

MARTY, Ph., TROMBETTA, P., AND GARANDET, J.P. Contrôle de la stabilité d'un écoulement thermoconvectif par un champ magnétique tournant *Comptes Rendus de l'Académie des Sciences, Paris, Série IIb*, t.326, p. 185-190, 1998.

MAZURUK, K., RAMACHANDRAN, N., VOLZ, M. and GILLIES, D. Study of frequency effects of a rotating magnetic field on fluid flow in vertical cylinders. *Soc. of Photo-optical Instrum. Eng.*, Vol.3123, San Diego, 1997.

PRIEDE, J. Theoretical study of a flow in an axisymmetric cavity of finite length, driven by a rotating magnetic field. *PhD thesis, Institute of Physics, Latvian Academy of Science*, Salaspils, 1993.

RICHARDSON, A.T. On the stability of a magnetically driven rotating fluid flow. *Journal of Fluid Mechanics*, 63:593–605, 1974.

SØRENSEN, J.N. and PHUOC LOC, TA.. High-order axisymmetric Navier-stokes code: Description and evaluation of boundary conditions. *International Journal For Numerical Methods In Fluids*, 9:1517–1537, 1989.

VILLERMAUX, E. On the role of viscosity in shear instabilities, *Physics of Fluids*, Vol. 10, n.2, 1998.

WALKER, J.S. Bridgman crystal growth with a strong, low-frequency, rotating magnetic field, *to appear in J. of Crystal Growth*, 1998.